# Flux Magnetism in a Strongly Interacting Dipolar Lattice Supersolid under Tunable Gauge Fields

# Flux Magnetism in a Strongly Interacting Dipolar Lattice Supersolid under Tunable Gauge Fields

Michele Miotto,[1,*] Pietro Lombardi,[2,3] Giovanni Ferioli,[4] Joana Fraxanet,[5] Maciej Lewenstein,[5,6] Luca Tanzi,[2,3] and Luca Barbiero[7,†]

[1]Institut für Physik und Astronomie, Technische Universität Berlin, Hardenbergstraße 36, 10623 Berlin, Germany
[2]Consiglio Nazionale delle Ricerche—Istituto Nazionale di Ottica, Sede Secondaria di Sesto Fiorentino
[3]European Laboratory for Nonlinear Spectroscopy (LENS), Università di Firenze, Firenze, Italy
[4]Department of Physics and Astronomy, University of Florence, 50019 Sesto Fiorentino, Italy
[5]ICFO—Institut de Ciencies Fotoniques, The Barcelona Institute of Science and Technology, Avinguda Carl Friedrich Gauss 3, 08860 Castelldefels (Barcelona), Spain
[6]ICREA, Passeig de Lluís Companys 23, 08010 Barcelona, Spain
[7]Institute for Condensed Matter Physics and Complex Systems, DISAT, Politecnico di Torino, I-10129 Torino, Italy

(Received 19 September 2025; revised 10 June 2026; accepted 12 June 2026; published 22 July 2026)

Supersolidity and magnetism are fundamental phenomena characterizing strongly correlated matter. Here we unveil a mechanism that directly connects these two regimes and can be experimentally accessed in ultracold atomic systems. Specifically, we exploit the distinctive properties of magnetic lanthanide atoms trapped in a one-dimensional antimagic wavelength optical lattice. This platform enables a realistic implementation of a triangular Bose-Hubbard ladder featuring two key ingredients: strong long-range interactions and tunable gauge fields. Owing to these properties, our numerical analysis reveals a robust lattice supersolid regime with finite fluxes in each triangular plaquette. Remarkably, we show that the density modulation of the supersolid phase and a finite gauge field induce magnetic ordering of the fluxes, forming ferromagnetic and ferrimagnetic patterns. Our results thus reveal a quantum effect that bridges supersolidity and magnetism.

DOI: 10.1103/tbp3-7rh3

*Introduction*—The quantum mechanical effects underlying the formation of strongly interacting states of matter represent a fundamental topic in quantum physics [1,2], yet key mechanisms remain unexplored. In this context, ultracold atomic systems [3–5] have emerged as an innovative tool to deepen the understanding of a wide variety of quantum many-body phases [6–9], among which magnetism [10,11] is a primary example. Evidence for this is provided by the remarkable realizations of ferromagnetic [12,13], antiferromagnetic [14,15], and ferrimagnetic [16] states, where specific atomic degrees of freedom effectively reproduce electron spin orderings.

The fundamental role played by trapped atoms at ultralow temperatures [17,18] has been further highlighted by the observation of one of the most elusive states of matter: supersolidity [19–21]. While first instances of this regime have been achieved in different setups [22–24], the anisotropic long-range dipolar interaction promoted magnetic lanthanide atoms [25] as the primary constituents of supersolid phases [26–28].

Great efforts have also been devoted to create strongly correlated phases driven by dipolar interactions in settings where magnetic atoms are trapped in optical lattices [29–32]. In this direction, important results have exploited a drastic reduction of the lattice spacing [30,33,34]. Nevertheless, accessing and probing these regimes remains highly challenging, and alternative strategies might be of crucial relevance.

In this Letter, we establish a connection between magnetism and supersolidity, which can be directly explored using an innovative experimental setup that significantly magnifies the long-range dipolar repulsion. In particular, we first design a configuration where magnetic dysprosium atoms are confined in a one-dimensional antimagic wavelength optical lattice, which enables two Zeeman states to occupy spatially shifted sublattices separated by $\lambda/4$–100 nm. Raman coupling [35–38] between spin states generates tunable complex tunneling processes across the sublattices, effectively synthesizing a triangular extended Bose-Hubbard ladder in a gauge field [39–44]. Crucially, at this subwavelength scale the dipolar interaction between nearest-neighbor sites becomes comparable to the on-site one in a broad range of lattice depths.

*Contact author: m.miotto@tu-berlin.de
†Contact author: luca.barbiero@polito.it

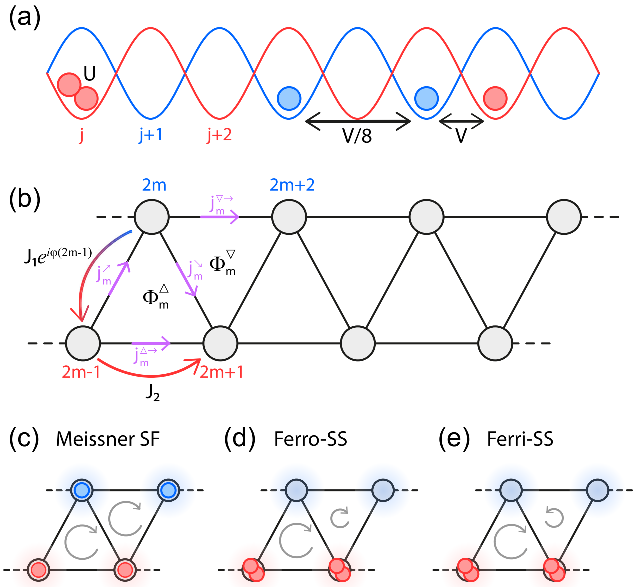


FIG. 1. (a) Two-component gas of Dy trapped in a one-dimensional optical lattice at the antimagic wavelength and relative interactions, see first row of Eq. (1). We note that the $\lambda/2$ periodicity of the intensity profile corresponds to $\Delta j = 2$. (b) Effective triangular ladder description of the model with correspondent hopping processes, see second and third rows of Eq. (1). Each triangular plaquette is characterized by effective current flux $\Phi_m^\Delta$ or $\Phi_m^\nabla$, see Eq. (5), with currents indicated in violet and defined in Eq. (6). (c)–(e) Local density and current flux patterns for the three observed phases in the case of explicitly broken time reversal symmetry.

Our numerical analysis reveals that, because of these intriguing features, interesting many-body phases, including a lattice supersolid [17,45–48], characterize the ground state of this system. Strikingly, this supersolid regime hosts staggered flux patterns with magnetic order—either ferromagnetic or ferrimagnetic—arising from the interplay between finite gauge fields and the dipolar repulsion induced density modulation. Finally, we provide a concrete procedure to prepare and probe the intriguing states of matter that our results unveil.

*Magnetic atoms in an antimagic wavelength optical lattice*—Our scheme builds on magnetic lanthanide atoms, such as dysprosium and erbium, confined in a one-dimensional optical lattice of wavelength $\lambda$. These atoms exhibit a large tensorial polarizability in the ground state due to their unfilled $4f$ shell, giving rise to strongly state-dependent optical potentials [34,49–52]. By exploiting the ability to tune the scalar-to-tensorial polarizability ratio near an electronic resonance, an antimagic potential [40,42] for two successive Zeeman states can be achieved. In this regime, the selected states experience optical potentials of equal depth and opposite sign [53], thus producing two spin-selective sublattices displaced by $\lambda/4$. Importantly, this enables interparticle spacings as small as 100 nm—well below standard optical lattice scales—without resorting to ultraviolet light [60,61]. We focus on bosonic dysprosium atoms in the Zeeman sublevels $|a\rangle = |J = 8, m_J = -8\rangle$ and $|b\rangle = |J = 8, m_J = -7\rangle$, which are particularly suitable as they exhibit suppressed dipolar relaxation and nearly equal contact interactions $U_{aa} \approx U_{bb} = U$ when the magnetic field is tuned near 2.75 G [62]. The antimagic condition for $|a\rangle$ and $|b\rangle$ is satisfied whenever the scalar and tensorial polarizabilities reach a specific ratio, which naturally occurs near electronic resonances [53]. In our scheme, this condition is fulfilled in the 529.87–530.25 nm range. Crucially, in this configuration the effective nearest-neighbor dipolar repulsion reaches $V/h \approx 130$ Hz, thus comparable to the on-site interaction $U$ across a wide range of lattice depths [53]. Note that similar dipole-dipole interaction strengths are obtained with polar molecules in lattices with ~0.5 μm spacing [63,64]. Coherent tunneling between the two spin states is induced by a two-photon Raman coupling [35,65], which drives spin-flip hopping between adjacent sites of the two sublattices. This process generates a complex nearest-neighbor tunneling term $J_1 e^{i\varphi}$, where the amplitude is set by the Raman intensity and spatial overlap between the initial and the final states, while the gauge field $\varphi$ is determined by the beam geometry [35–38]. In contrast, next-nearest-neighbor tunneling $J_2$ arises from kinetic processes within each sublattice and is controlled by the lattice depth. The resulting system is described by the extended Bose-Hubbard Hamiltonian

$$H = \sum_{j=1}^{L}\left[V\sum_{k>j}^{L}\frac{n_j n_k}{(k-j)^3} + \frac{U}{2}n_j(n_j-1)\right] - \sum_{m=1}^{(L-2)/2}\left[J_2\left(a_{2m-1}^\dagger a_{2m+1} + a_{2m}^\dagger a_{2m+2} + \text{H.c.}\right) + J_1\left(e^{\imath\varphi(2m-1)}a_{2m-1}^\dagger a_{2m} + e^{-\imath\varphi(2m)}a_{2m}^\dagger a_{2m+1} + \text{H.c.}\right)\right]. \tag{1}$$

Notably, although our approach relies on a purely one-dimensional trapping potential, Eq. (1) effectively describes a strongly interacting triangular ladder in a gauge, see Fig. 1. More in detail, here $a^\dagger$ and $a$ are the usual bosonic operators. For ease of notation, the index $m$ runs over the effective triangular plaquettes and is shared by two consecutive plaquettes, while $j$ and $k$ run over all $L$ lattice sites. The specific structure of the nearest-neighbor hopping term leads to triangular plaquettes being pierced by a gauge field of $\pm\varphi$. In the following sections, we employ the density-matrix renormalization group (DMRG) method [66–68] to investigate the possible quantum phases emerging from the distinctive properties of $H$.

*Geometrically frustrated regime* ($\varphi = \pi$)—We begin our analysis by fixing $\varphi = \pi$ and the particle density $\bar{n} = [(N_a + N_b)/L] = 1$. Notably, this choice generates a

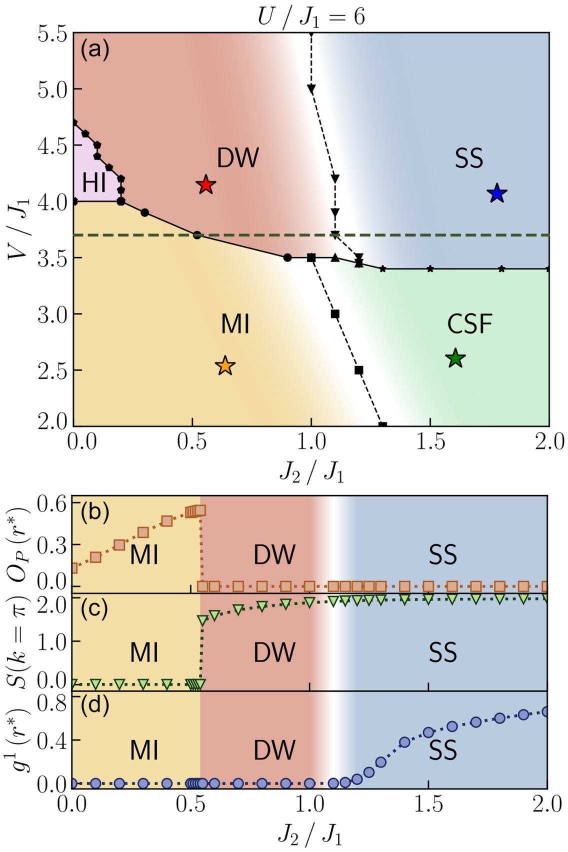


FIG. 2. (a) Phase diagram of the model in Eq. (1) at $\varphi = \pi$ and $U/J_1 = 6$, as a function of $V/J_1$ and $J_2/J_1$ for total density $\bar{n} = 1$. Here, we observe five different phases: MI, HI, DW, CSF, and SS. The stars refer to concrete experimental parameters, see Supplemental Material [53] for details, giving rise to the indicated values of $J_2/J_1$, $U/J_1$, $V/J_1$ and $\varphi$. Dashed lines and color gradients signal transitions of the KT type, while solid lines indicate first-order transitions. The horizontal dashed line at $V/J_1 = 3.7$ represents the cut along which the order parameters are shown in the panels below. (b) Parity operator (2) as a function of $J_2/J_1$, computed at $r^* = 200$. (c) Structure factor (3) for $k = \pi$ as a function of $J_2/J_1$. (d) Expectation value of $g^1$ (4) as a function of $J_2/J_1$, computed at $r^* = 200$. In the DMRG simulations, we used maximum bond dimension $\chi = 800$.

sign staggered real-valued $J_1$, which, for finite $J_2$, can induce effective geometric frustration [41,42,69–74]. Our results in Fig. 2(a) show that for small $J_2/J_1$ the frustration is not effective and Eq. (1) reproduces the phase diagram of the widely investigated frustration-free 1D extended Bose-Hubbard model [45,61,75–79]. In this regime, dominant onsite repulsions $U$ stabilize a Mott insulator (MI), captured by the parity order parameter [80,81]

$$O_P(r) = e^{i\pi \sum_{j<r} \delta n_j} \tag{2}$$

with $\delta n_j = (\bar{n} - n_j)$, see Fig. 2(b). By increasing $V$, the MI is replaced by the topological Haldane insulator (HI), while for even stronger dipolar repulsions, a density wave (DW) insulator emerges. In the latter, the translational symmetry breaks down and alternation between sites with high and low occupation occurs. As is intuitive, this density modulation is captured by a finite peak at $k = \pi$ in the structure factor

$$S(k) = \frac{1}{L} \sum_r e^{-\imath kr} \langle n_j n_{j+r} \rangle. \tag{3}$$

Importantly, increasing geometric frustration, i.e., taking larger $J_2/J_1$ ratios, profoundly alters this picture. Specifically, for low $V$ the MI undergoes a transition of the Kosterlitz-Thouless (KT) type and is replaced by a chiral superfluid (CSF) [53] with spontaneously broken time-reversal symmetry [41,42,71,72,74,82]. In Fig. 2(a), see the horizontal dashed line, we further find that for larger dipolar repulsions, geometric frustration can induce a first-order phase transition from a Mott insulating to a density wave regime. Evidence of this is reported in Figs. 2(b) and 2(c), where we show that at a critical value $J_2/J_1$ the parity operator $O_P(r)$ vanishes and the finite value $S(k = \pi)$ signals the breaking of the translational symmetry. As shown in Fig. 2(d), important information can also be extracted from the behavior of the single particle Green function

$$g^1(|k - j|) = \langle b_k^\dagger b_j \rangle \tag{4}$$

for finite large distances $|k - j|$. In both MI and DW, $g^1(|k - j|) \approx 0$ already for relatively short distances, indicating an exponential decay distinctive of insulating phases. In contrast, by increasing $J_2/J_1$ the single particle Green function decays algebraically and its value for large $|k - j|$ becomes significant. According to Luttinger theory [83], this behavior signals the onset of a one dimensional gapless superfluid (SF) phase. Crucially, in this regime $S(\pi) \neq 0$, indicating that superfluidity coexists with the breaking of the translational symmetry. As a consequence, these results define a lattice supersolid (SS) phase. The DW-SS transition is also of the KT type, analogous to the MI-SF transition observed in the conventional 1D Bose-Hubbard model [84]. It is important to emphasize that, in the regimes of relatively large $U$, this SS phase cannot take place if either $J_2 \approx 0$ or $V \approx 0$. This highlights that the combination of geometric frustration and large dipolar repulsions is responsible for the appearance of this $\bar{n} = 1$ lattice SS phase.

*Magnetic ordering of fluxes*—Except for a few known examples [85,86], SS states typically preserve time-reversal invariance. Here, the tunability of the gauge field enables us to systematically investigate the properties of supersolidity under explicitly broken time-reversal symmetry. Important insight on this latter scenario can be also unveiled through the behavior of the generated current flux in odd and even effective triangular plaquettes

$$\Phi_m^{\triangle} = j_m^{\nearrow} + j_m^{\searrow} - j_m^{\triangle\rightarrow},$$
$$\Phi_m^{\triangledown} = -j_{m+1}^{\nearrow} - j_m^{\searrow} + j_m^{\triangledown\rightarrow}, \tag{5}$$

respectively, where

$$j_m^{\nearrow} = -\imath J_1\left(e^{\imath\varphi(2m-1)}a_{2m-1}^{\dagger}a_{2m} - \text{H.c.}\right),$$
$$j_m^{\searrow} = -\imath J_1\left(e^{-\imath\varphi(2m)}a_{2m}^{\dagger}a_{2m+1} - \text{H.c.}\right),$$
$$j_m^{\triangle\rightarrow} = -\imath J_2\left(a_{2m-1}^{\dagger}a_{2m+1} - \text{H.c.}\right),$$
$$j_m^{\triangledown\rightarrow} = -\imath J_2\left(a_{2m}^{\dagger}a_{2m+2} - \text{H.c.}\right) \tag{6}$$

are the currents along the diagonal and horizontal links, see Fig. 1(b), and the overall staggered flux average [87]

$$\bar{\Phi} = \sum_{m=1}^{(L-3)/2} (\Phi_m^{\triangle} - \Phi_m^{\triangledown})/(L-3). \tag{7}$$

In our analysis, we fix the Hamiltonian parameters $U$, $V$, $J_1$, and $J_2$ able to stabilize the SS regime illustrated in Fig. 2(a), and explore the effects produced by variations of the gauge field in the range $0 < \varphi < \pi$. In Fig. 3(a), we report that, for a weak $\varphi$, superfluidity—signaled by $g^1(r^*) \neq 0$—persists, while the vanishing $S(\pi)$ in Fig. 3(b) indicates that translational invariance is preserved [88]. Therefore, we can conclude that supersolidity is unstable for small gauge fields and a homogeneous superfluid emerges as the favorable ground state. We now exploit the similarity between the periodic structures that $\Phi_m^{\triangle}/\Phi_m^{\triangledown}$ can develop and the magnetic ordering of spins in the odd/even sites of a 1D chain with effective staggered magnetization $\bar{\Phi}$. Based on this, the results in Figs. 3(c) and 3(d) find this SF phase, usually called Meissner SF [41,89,90], to be characterized by an effective ferromagnetic flux structure as $\Phi_m^{\triangle} = \Phi_m^{\triangledown} > 0$ and $\bar{\Phi} = 0$, see also Supplemental Material [53]. By increasing $\varphi$, different flux magnetic orderings emerge. Specifically, Figs. 3(a) and 3(b) report that for $\varphi \geq 0.18\pi$ both $g^1(r^*)$ and $S(\pi)$ are finite, thus a first-order transition related to the spontaneous breaking of the translation symmetry occurs and a SS state takes place. Figure 3(c) further explains that this SS phase features an average staggered flux $\bar{\Phi} > 0$ that signals the asymmetric alternation between $\Phi_m^{\triangle}$ and $\Phi_m^{\triangledown}$. Importantly, this latter condition is induced by the presence of a finite gauge field and by the SS density structure. Indeed, the density imbalance between the legs causes the emergence of finite interleg current, which is equal along all diagonal links $j_m^{\nearrow} = j_m^{\searrow}$. Furthermore, the high/low occupation of odd/even sites implies $|j_m^{\triangle\rightarrow}| > |j_m^{\triangledown\rightarrow}|$ [53]. These facts, together with $j_m^{\triangle\rightarrow} < 0$, lead to $\Phi_m^{\triangle} > \Phi_m^{\triangledown} > 0$ [91] in this range of parameters, see Fig. 3(e). As a consequence, we can identify such a phase as a supersolid characterized by a

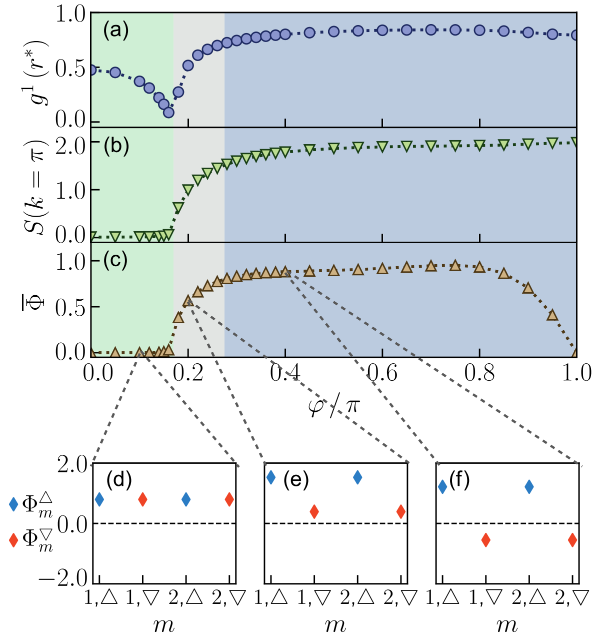


FIG. 3. Behavior of (a) the single particle Green function $g^1$ at $r^* = 60$; (b) the structure factor $S(\pi)$; (c) the overall staggered flux average $\bar{\Phi}$, as a function of $\varphi/\pi$ and fixed $U/J_1 = 6$, $V/J_1 = 4.5$ and $J_2/J_1 = 1.7$. Green regions correspond to the Meissner superfluid, while grey and violet areas indicate ferro- and ferrimagnetic supersolid phases, respectively. Panels (d)–(f) show the effective current fluxes per plaquette $\Phi_m^{\triangle}$ and $\Phi_m^{\triangledown}$ for $\varphi/\pi = \{0.1, 0.2, 0.4\}$, respectively. The plaquettes are taken in the middle of the chain of length $L = 101$. In the DMRG simulations, we used maximum bond dimension $\chi = 1000$. We have checked that the values of the currents entering the equations for $\Phi_m^{\triangle}$ and $\Phi_m^{\triangledown}$ are robust against changes of the length of the chain.

ferromagnetic flux structure (Ferro-SS). For larger $\varphi$, our numerics show that the density modulation of the SS phase still enables the appearance of a staggered flux pattern. Importantly, we observe a crossover to the conditions $\Phi_m^{\triangle} > 0 > \Phi_m^{\triangledown}$ and $|\Phi_m^{\triangle}| > |\Phi_m^{\triangledown}|$ being fulfilled, as shown in Fig. 3(f). In analogy with spin chains, this structure thus describes a ferrimagnetic flux ordering embedded in a SS phase (Ferri-SS). These results thus unveil that intriguing states of matter—the Ferro-SS and Ferri-SS phases—where supersolidity and magnetism coexist can characterize strongly correlated regimes. Importantly, these unconventional features emerge thanks to the specific density structure of a lattice SS phase combined with large enough gauge fields.

*State preparation and detection scheme*—Here, we show how these many-body phases can be experimentally prepared and probed with high accuracy. Specifically, the ground state of the Hamiltonian equation (1) can be prepared by directly loading a Dy Bose-Einstein condensate in the $|8,-8\rangle$ state into the antimagic optical lattice. With an appropriate tuning of interatomic interaction and axial confinement, the system can be initialized in a low-energy, doubly occupied, Mott insulator phase. Adiabatically turning on the Raman coupling induces a finite occupation of the $|8,-7\rangle$ state [53], thereby enabling access to the unit-filling regime $\bar{n}=1$. Moreover, as accurately shown in [53] and reported in Fig. 2(a), by exploiting the possibility to independently tune all the Hamiltonian parameters $J_1$, $\varphi$, $J_2$, $U$, and $V$, the discussed regimes turn out to be experimentally accessible. Taking advantage also of the synthetic nature of the ladder geometry, such states of matter can be detected in the experiment using standard spin-resolved time-of-flight (TOF) absorption imaging, without the need for a quantum gas microscope and single-site resolution. Indeed, TOF images provide information about the momentum distribution of the atomic sample in the lattice. On the one hand, this measurement gives access to the single-particle Green function $g^1(r)$ [92], thus distinguishing phases with superfluid properties (SF and SS) from insulators (MI and DW). On the other hand, by performing state-sensitive imaging, e.g., by applying a magnetic field gradient during the free expansion, one can differentiate between phases characterized by mainly one spin component (SS and DW) and phases characterized by two equally populated spin components (SF and MI). To detect the different magnetic orderings appearing in the SS regime, an investigation of the currents in both the real and the synthetic dimensions is required. A simple measurement in state resolved band-mapping procedure is enough to determine the presence of collective currents in the real one [37]. Concerning the synthetic direction, following [93], we propose to project the ladder system onto a 1D lattice of isolated double wells in the synthetic dimension, each well corresponding to a spin state, and use the complex hopping $J_1$ induced by the Raman transition to map the current operator between the two wells onto the double-well population imbalance, see Supplemental Material [53].

*Conclusions and perspectives*—Our results unveil a mechanism linking supersolidity and magnetism. Thanks to the capability of achieving strong dipolar repulsions in the presence of tunable gauge fields, our derived experimental setup offers a direct path to probe such a scenario as well as to explore strongly correlated regimes dominated by long-range interactions. As we prove, these configurations can be realistically achieved by exploiting the properties of Raman coupled magnetic lanthanide atoms trapped in an optical lattice at the antimagic wavelength. Motivated by the versatility offered by this innovative setup, our numerical analysis reveal that the interplay of tunable gauge fields and large local and long-range interactions makes possible the appearance of a lattice supersolid phase where fluxes order into ferromagnetic or ferrimagnetic structures.

From an experimental perspective, our results provide a powerful and alternative strategy to magnify the strength of the dipolar interaction in lattice systems without resorting to UV wavelengths [60,61] or bilayer lattice schemes [34]. The further tunability of gauge fields, makes it possible to envision our setup as an important future tool for exploring strongly interacting phases of matter in effective magnetic fields, whose quantum simulation represents a challenging and timely research subject [90,94]. In addition, because of the controlled spin state occupation, this architecture can be further employed to engineer Hamiltonians in constrained spin space [62,95,96]. We finally remark that, although we concentrated on dysprosium, our scheme directly applies to erbium.

From a theory perspective, a natural question concerns the possible existence of similar linking mechanisms between different strongly correlated states of matter. In addition, an important future direction will be to explore whether similar flux orderings emerge in 2D lattices, where supersolidity is also predicted [97]. Importantly, magnetically ordered fluxes in 2D can also suggest the presence of topologically protected phases [98]. As a consequence, our results might represent a first preliminary step to reveal a possible connection between supersolidity and topology.

Our results provide a new avenue to create and understand many-body regimes dominated by long-range interactions and reveal an intriguing interplay between supersolidity and magnetism.

Calculations were performed using the TeNPy library (version 1.0.0) [68].

*Acknowledgments*—We thank N. Baldelli, C. Cabrera, S. Dhar, A. Eckardt, F. Ferlaino, M. Landini, M. Mark, G. Modugno, L. Santos, and G. Valtolina for discussions. M. M., L. T., and L. B. acknowledge funding from the Italian MUR (PRIN DiQut Grant No. 2022523NA7). M. M. acknowledges funding from the Deutsche Forschungs gemeinschaft (DFG, German Research Foundation) via the Research Unit FOR 5688 (Project No. 521530974). P. L., G. F., and L. T. acknowledge funding from the European Union (European Research Council, SUPERSOLIDS, Grant No. 101055319). M. L. acknowledges support from: European Research Council AdG NOQIA; MCIN/AEI [PGC2018-0910.13039/501100011033, CEX2019000910-S/10.13039/501100011033, Plan National FIDEUA PID2019–106901 GB-I00, Plan National STAMEENA PID2022-139099NB I00, project funded by MCIN/AEI/10.13039/501100011033 and by the "European Union NextGenerationEU/PRTR"; (PRTRC17.I1), FPI]; QUANTERA DYNAMITE PCI2022132919, the QuantERA II Programme cofunded by European Union's Horizon 2020 program under Grant Agreement No. 101017733; the Ministry for Digital Transformation and of Civil Service of the Spanish Government through the QUANTUM ENIA project call—Quantum Spain project, and by the European Union through the Recovery, Transformation and Resilience Plan NextGenerationEU within the framework of the Digital Spain 2026 Agenda; Fundació Cellex; Fundació Mir-Puig; Generalitat de

Catalunya, European Social Fund FEDER and CERCA program; Barcelona Supercomputing Center MareNostrum (FI-2023-3-0024); funded by the European Union; HORIZON-CL4-2022-QUANTUM-02-SGA PASQuan-S2.1, 101113690, EU Horizon 2020 FETOPEN OPTOlogic, Grant No. 899794, QU-ATTO, 101168628, the EU Horizon Europe Program (this project has received funding from the European Union's Horizon Europe research and innovation program under Grant Agreement No. 101080086 NeQST, Grant Agreement No. 101080086 —NeQST); ICFO Internal "QuantumGaudi" project.

Views and opinions expressed are however those of the author(s) only and do not necessarily reflect those of the European Union, European Commission, European Climate, Infrastructure and Environment Executive Agency (CINEA), or any other granting authority. Neither the European Union nor any granting authority can be held responsible for them.

*Data availability*—The data that support the findings of this article are openly available [99].

[1] D. J. Thouless, *The Quantum Mechanics of Many-Body Systems* (Courier Corporation, Mineola, NY, 2013).
[2] S. M. Girvin and K. Yang, *Modern Condensed Matter Physics* (Cambridge University Press, Cambridge, England, 2019).
[3] M. Lewenstein, A. Sanpera, V. Ahufinger, B. Damski, A. Sen (De), and U. Sen, Adv. Phys. **56**, 243 (2007).
[4] M. Lewenstein, A. Sanpera, and V. Ahufinger, *Ultracold Atoms in Optical Lattices: Simulating Quantum Many-Body Systems* (Oxford University Press, Oxford, 2012).
[5] C. Gross and I. Bloch, Science **357**, 995 (2017).
[6] N. Goldman, J. C. Budich, and P. Zoller, Nat. Phys. **12**, 639 (2016).
[7] J. Argüello-Luengo, A. González-Tudela, T. Shi, P. Zoller, and J. I. Cirac, Nature (London) **574**, 215 (2019).
[8] D.-W. Zhang, Y.-Q. Zhu, Y. X. Zhao, H. Yan, and S.-L. Zhu, Adv. Phys. **67**, 253 (2018).
[9] M. Aidelsburger *et al.*, Phil. Trans. R. Soc. A **380**, 20210064 (2022).
[10] K. H. J. Buschow and F. R. de Boer, *Physics of Magnetism and Magnetic Materials*, Focus on Biotechnology (Springer US, New York, 2003).
[11] A. Auerbach, *Interacting Electrons and Quantum Magnetism*, Graduate Texts in Contemporary Physics (Springer, New York, 2012).
[12] C. V. Parker, L.-C. Ha, and C. Chin, Nat. Phys. **9**, 769 (2013).
[13] R. Cominotti, A. Berti, C. Dulin, C. Rogora, G. Lamporesi, I. Carusotto, A. Recati, A. Zenesini, and G. Ferrari, Phys. Rev. X **13**, 021037 (2023).
[14] A. Mazurenko, C. S. Chiu, G. Ji, M. F. Parsons, M. Kanász-Nagy, R. Schmidt, F. Grusdt, E. Demler, D. Greif, and M. Greiner, Nature (London) **545**, 462 (2017).
[15] H.-J. Shao, Y.-X. Wang, D.-Z. Zhu, Y.-S. Zhu, H.-N. Sun, S.-Y. Chen, C. Zhang, Z.-J. Fan, Y. Deng, X.-C. Yao *et al.*, Nature (London) **632**, 267 (2024).
[16] M. Lebrat, A. Kale, L. H. Kendrick, M. Xu, Y. Gang, A. Nikolaenko, P. M. Bonetti, S. Sachdev, and M. Greiner, Science **392**, 612 (2026).
[17] K. Góral, L. Santos, and M. Lewenstein, Phys. Rev. Lett. **88**, 170406 (2002).
[18] A. Recati and S. Stringari, Nat. Rev. Phys. **5**, 735 (2023).
[19] A. F. Andreev and I. M. Lifshitz, Sov. Phys. JETP **29**, 1107 (1969), http://www.jetp.ras.ru/cgi-bin/e/index/e/29/6/p1107?a=list.
[20] G. V. Chester, Phys. Rev. A **2**, 256 (1970).
[21] A. J. Leggett, Phys. Rev. Lett. **25**, 1543 (1970).
[22] J.-R. Li, J. Lee, W. Huang, S. Burchesky, B. Shteynas, F. Ç. Top, A. O. Jamison, and W. Ketterle, Nature (London) **543**, 91 (2017).
[23] J. Léonard, A. Morales, P. Zupancic, T. Esslinger, and T. Donner, Nature (London) **543**, 87 (2017).
[24] C. S. Chisholm, S. Hirthe, V. B. Makhalov, R. Ramos, R. Vatré, J. Cabedo, A. Celi, and L. Tarruell, Science **391**, 480 (2026).
[25] L. Chomaz, I. Ferrier-Barbut, F. Ferlaino, B. Laburthe-Tolra, B. L. Lev, and T. Pfau, Rep. Prog. Phys. **86**, 026401 (2022).
[26] L. Tanzi, S. M. Roccuzzo, E. Lucioni, F. Famà, A. Fioretti, C. Gabbanini, G. Modugno, A. Recati, and S. Stringari, Nature (London) **574**, 382 (2019).
[27] M. Guo, F. Böttcher, J. Hertkorn, J.-N. Schmidt, M. Wenzel, H. P. Büchler, T. Langen, and T. Pfau, Nature (London) **574**, 386 (2019).
[28] L. Chomaz, D. Petter, P. Ilzhöfer, G. Natale, A. Trautmann, C. Politi, G. Durastante, R. M. W. van Bijnen, A. Patscheider, M. Sohmen, M. J. Mark, and F. Ferlaino, Phys. Rev. X **9**, 021012 (2019).
[29] A. de Paz, A. Sharma, A. Chotia, E. Maréchal, J. H. Huckans, P. Pedri, L. Santos, O. Gorceix, L. Vernac, and B. Laburthe-Tolra, Phys. Rev. Lett. **111**, 185305 (2013).
[30] S. Baier, M. J. Mark, D. Petter, K. Aikawa, L. Chomaz, Z. Cai, M. Baranov, P. Zoller, and F. Ferlaino, Science **352**, 201 (2016).
[31] S. Lepoutre, J. Schachenmayer, L. Gabardos, B. Zhu, B. Naylor, E. Maréchal, O. Gorceix, A. M. Rey, L. Vernac, and B. Laburthe-Tolra, Nat. Commun. **10**, 1714 (2019).
[32] A. Patscheider, B. Zhu, L. Chomaz, D. Petter, S. Baier, A.-M. Rey, F. Ferlaino, and M. J. Mark, Phys. Rev. Res. **2**, 023050 (2020).
[33] L. Su, A. Douglas, M. Szurek, R. Groth, S. F. Ozturk, A. Krahn, A. H. Hébert, G. A. Phelps, S. Ebadi, S. Dickerson, F. Ferlaino, O. Marković, and M. Greiner, Nature (London) **622**, 724 (2023).
[34] L. Du, P. Barral, M. Cantara, J. de Hond, Y.-K. Lu, and W. Ketterle, Science **384**, 546 (2024).
[35] Y. J. Lin, K. Jiménez-García, and I. B. Spielman, Nature (London) **471**, 83 (2011).
[36] A. Celi, P. Massignan, J. Ruseckas, N. Goldman, I. B. Spielman, G. Juzeliūnas, and M. Lewenstein, Phys. Rev. Lett. **112**, 043001 (2014).
[37] M. Mancini, G. Pagano, G. Cappellini, L. Livi, M. Rider, J. Catani, C. Sias, P. Zoller, M. Inguscio, M. Dalmonte, and L. Fallani, Science **349**, 1510 (2015).

[38] B. K. Stuhl, H.-I. Lu, L. M. Aycock, D. Genkina, and I. B. Spielman, Science **349**, 1514 (2015).
[39] J. Struck, M. Weinberg, C. Ölschläger, P. Windpassinger, J. Simonet, K. Sengstock, R. Höppner, P. Hauke, A. Eckardt, M. Lewenstein, and L. Mathey, Nat. Phys. **9**, 738 (2013).
[40] E. Anisimovas, M. Račiūnas, C. Sträter, A. Eckardt, I. B. Spielman, and G. Juzeliūnas, Phys. Rev. A **94**, 063632 (2016).
[41] C.-M. Halati and T. Giamarchi, Phys. Rev. Res. **5**, 013126 (2023).
[42] N. Baldelli, C. R. Cabrera, S. Julià-Farré, M. Aidelsburger, and L. Barbiero, Phys. Rev. Lett. **132**, 153401 (2024).
[43] T. Chanda, L. Barbiero, M. Lewenstein, M. J. Mark, and J. Zakrzewski, Rep. Prog. Phys. **88**, 044501 (2025).
[44] Y. Li, H. Cai, D. W. Wang, L. Li, J. Yuan, and W. Li, Phys. Rev. Lett. **124**, 140401 (2020).
[45] G. G. Batrouni, R. T. Scalettar, V. G. Rousseau, and B. Grémaud, Phys. Rev. Lett. **110**, 265303 (2013).
[46] Y. Li, L. He, and W. Hofstetter, Phys. Rev. A **87**, 051604 (2013).
[47] T. Mishra, S. Greschner, and L. Santos, Phys. Rev. A **91**, 043614 (2015).
[48] R. Kraus, T. Chanda, J. Zakrzewski, and G. Morigi, Phys. Rev. B **106**, 035144 (2022).
[49] H. Li, J.-F. Wyart, O. Dulieu, S. Nascimbène, and M. Lepers, J. Phys. B **50**, 014005 (2017).
[50] J. H. Becher, S. Baier, K. Aikawa, M. Lepers, J.-F. Wyart, O. Dulieu, and F. Ferlaino, Phys. Rev. A **97**, 012509 (2018).
[51] T. Chalopin, V. Makhalov, C. Bouazza, A. Evrard, A. Barker, M. Lepers, J.-F. Wyart, O. Dulieu, J. Dalibard, R. Lopes, and S. Nascimbene, Phys. Rev. A **98**, 040502(R) (2018).
[52] D. Bloch, B. Hofer, S. R. Cohen, A. Browaeys, and I. Ferrier-Barbut, Phys. Rev. Lett. **131**, 203401 (2023).
[53] See Supplemental Material http://link.aps.org/supplemental/10.1103/tbp3-7rh3 for a precise derivation of the antimagic optical lattice condition, tunability of the Hamiltonian parameters, the detection schemes for the quantities defined in the text, characterization of the chiral superfluid phase, and calculation of the flux patterns. The Supplemental Material includes Refs. [54–59].
[54] M. Lepers, J.-F. Wyart, and O. Dulieu, Phys. Rev. A **89**, 022505 (2014).
[55] V. A. Dzuba, V. V. Flambaum, and B. L. Lev, Phys. Rev. A **83**, 032502 (2011).
[56] D. Bloch, B. Hofer, S. R. Cohen, M. Lepers, A. Browaeys, and I. Ferrier-Barbut, Phys. Rev. A **110**, 033103 (2024).
[57] B. Pasquiou, E. Maréchal, G. Bismut, P. Pedri, L. Vernac, O. Gorceix, and B. Laburthe-Tolra, Phys. Rev. Lett. **106**, 255303 (2011).
[58] N. Q. Burdick, K. Baumann, Y. Tang, M. Lu, and B. L. Lev, Phys. Rev. Lett. **114**, 023201 (2015).
[59] M. Gall, N. Wurz, J. Samland, C. F. Chan, and M. Köhl, Nature (London) **589**, 40 (2021).
[60] M. Sohmen, M. J. Mark, M. Greiner, and F. Ferlaino, SciPost Phys. **15**, 182 (2023).
[61] J. Fraxanet, D. González-Cuadra, T. Pfau, M. Lewenstein, T. Langen, and L. Barbiero, Phys. Rev. Lett. **128**, 043402 (2022).
[62] M. Lecomte, A. Journeaux, J. Veschambre, J. Dalibard, and R. Lopes, Phys. Rev. Lett. **134**, 013402 (2025).
[63] L. Christakis, J. S. Rosenberg, R. Raj, S. Chi, A. Morningstar, D. A. Huse, Z. Z. Yan, and W. S. Bakr, Nature (London) **614**, 64 (2023).
[64] A. N. Carroll, H. Hirzler, C. Miller, D. Wellnitz, S. R. Muleady, J. Lin, K. P. Zamarski, R. R. W. Wang, J. L. Bohn, A. M. Rey, and J. Ye, Science **388**, 381 (2025).
[65] N. Q. Burdick, Y. Tang, and B. L. Lev, Phys. Rev. X **6**, 031022 (2016).
[66] S. R. White, Phys. Rev. Lett. **69**, 2863 (1992).
[67] U. Schollwöck, Ann. Phys. (Amsterdam) **326**, 96 (2011).
[68] J. Hauschild *et al.*, SciPost Phys. Codebases 41 (2024).
[69] A. Eckardt, P. Hauke, P. Soltan-Panahi, C. Becker, K. Sengstock, and M. Lewenstein, Europhys. Lett. **89**, 10010 (2010).
[70] J. Cabedo, J. Claramunt, J. Mompart, V. Ahufinger, and A. Celi, Eur. Phys. J. D **74**, 123 (2020).
[71] S. Singha Roy, L. Carl, and P. Hauke, Phys. Rev. B **106**, 195158 (2022).
[72] L. Barbiero, J. Cabedo, M. Lewenstein, L. Tarruell, and A. Celi, Phys. Rev. Res. **5**, L042008 (2023).
[73] C.-M. Halati and T. Giamarchi, Phys. Rev. Res. **7**, 013199 (2025).
[74] D. Burba, G. Juzeliūnas, I. B. Spielman, and L. Barbiero, Commun. Phys. **8**, 141 (2025).
[75] E. G. Dalla Torre, E. Berg, and E. Altman, Phys. Rev. Lett. **97**, 260401 (2006).
[76] X. Deng and L. Santos, Phys. Rev. B **84**, 085138 (2011).
[77] D. Rossini and R. Fazio, New J. Phys. **14**, 065012 (2012).
[78] S. Ejima and H. Fehske, Phys. Rev. B **91**, 045121 (2015).
[79] K. Kottmann, P. Huembeli, M. Lewenstein, and A. Acín, Phys. Rev. Lett. **125**, 170603 (2020).
[80] E. Berg, E. G. Dalla Torre, T. Giamarchi, and E. Altman, Phys. Rev. B **77**, 245119 (2008).
[81] M. Endres, M. Cheneau, T. Fukuhara, C. Weitenberg, P. Schauß, C. Gross, L. Mazza, M. C. Bañuls, L. Pollet, I. Bloch, and S. Kuhr, Science **334**, 200 (2011).
[82] A. Dhar, M. Maji, T. Mishra, R. V. Pai, S. Mukerjee, and A. Paramekanti, Phys. Rev. A **85**, 041602 (2012).
[83] T. Giamarchi, *Quantum Physics in One Dimension* (Oxford University Press, New York, 2004).
[84] T. D. Kühner, S. R. White, and H. Monien, Phys. Rev. B **61**, 12474 (2000).
[85] W. Han, X.-F. Zhang, D.-S. Wang, H.-F. Jiang, W. Zhang, and S.-G. Zhang, Phys. Rev. Lett. **121**, 030404 (2018).
[86] O. M. Yevtushenko and A. M. Tsvelik, Phys. Rev. B **98**, 081118 (2018).
[87] For a triangular ladder with $L$ sites, the sum of $\triangle$ and $\bigtriangledown$ plaquettes is $L-2$. Furthermore, the ground state of the lattice SS phase is twofold degenerate, reflecting the equal probability of having high occupations in even or odd sites. Since we chose $L$ to be odd in order to lift this degeneracy, we exclude a plaquette in the calculation: this allows us to consider the same number of $\triangle$ and $\bigtriangledown$ plaquettes, thus justifying the factor $L-3$ in Eq. (7).
[88] Here we find only $S(k=0)\neq 0$, consistent with a homogeneous superfluid.

[89] M. Piraud, F. Heidrich-Meisner, I. P. McCulloch, S. Greschner, T. Vekua, and U. Schollwöck, Phys. Rev. B **91**, 140406 (2015).

[90] A. Impertro, S. Huh, S. Karch, J. F. Wienand, I. Bloch, and M. Aidelsburger, Nat. Phys. **21**, 895 (2025).

[91] In the text we selected the configuration favoring high occupation in odd sites, while the opposite one would imply $|j_m^{\triangle\rightarrow}| < |j_m^{\triangledown\rightarrow}|$ and therefore $|\Phi_m^{\triangle\rightarrow}| < |\Phi_m^{\triangledown\rightarrow}|$.

[92] M. Greiner, O. Mandel, T. Esslinger, T. Hänsch, and I. Bloch, Nature (London) **415**, 39 (2002).

[93] A. Impertro, S. Karch, J. F. Wienand, S. Huh, C. Schweizer, I. Bloch, and M. Aidelsburger, Phys. Rev. Lett. **133**, 063401 (2024).

[94] T.-W. Zhou, G. Cappellini, D. Tusi, L. Franchi, J. Parravicini, C. Repellin, S. Greschner, M. Inguscio, T. Giamarchi, M. Filippone, J. Catani, and L. Fallani, Science **381**, 427 (2023).

[95] F. Claude, L. Lafforgue, J. J. A. Houwman, M. J. Mark, and F. Ferlaino, Phys. Rev. Res. **6**, L042016 (2024).

[96] A. Douglas, V. Kaxiras, L. Su, M. Szurek, V. Singh, O. Marković, and M. Greiner, Phys. Rev. X **15**, 041021 (2025).

[97] B. Capogrosso-Sansone, C. Trefzger, M. Lewenstein, P. Zoller, and G. Pupillo, Phys. Rev. Lett. **104**, 125301 (2010).

[98] G. Giuliani and G. Vignale, Meaning of the highest occupied Kohn–Sham eigenvalue in metals, in *Quantum Theory of the Electron Liquid* (Cambridge University Press, Cambridge, England, 2005), pp. 717–718.

[99] M. Miotto, P. Lombardi, G. Ferioli, J. Fraxanet, M. Lewenstein, L. Tanzi, and L. Barbiero, Flux magnetism in a strongly interacting dipolar lattice supersolid under tunable gauge fields, (1.0) [Data set], Zenodo, 10.5281/zenodo.20848635 (2026).